Learning-based Surface Deformation Recovery for Large Radio Telescope Antennas: supplemental document

This document provides supplementary information to "Learning-based Surface Deformation Recovery for Large Radio Telescope Antennas". Here, we introduce the derivation of the mapping relationship between the distortion on the main reflector and the phase part of the wavefield on the aperture plane. In addition, the comparison of the RCNN model with and without pre-training is presented. Finally, the robustness of the RCNN model to the Poisson noise is investigated.

1. DERIVATION OF EQ. (1) IN THE MAIN TEXT

As shown in Fig. S1, given the normal surface error P*P, the corresponding optical path difference $\Delta l(x,y)$ can be written by

$$\begin{aligned}\Delta l(x,y) = \mathrm{MP} + \mathrm{PN} &\approx \frac{\delta(x,y)}{\cos\theta} + \frac{\delta(x,y)}{\cos\theta}\cdot\cos 2\theta \\ &= 2\delta(x,y)\cos\theta,\end{aligned} \tag{S1}$$

substituting $\phi(x,y) = (2\pi/\lambda)\Delta l(x,y)$ and $\cos\theta = 1/\sqrt{(1+\frac{x^2+y^2}{4f^2})}$ into Eq. (S1), we can get Eq. (1) in the mian text.

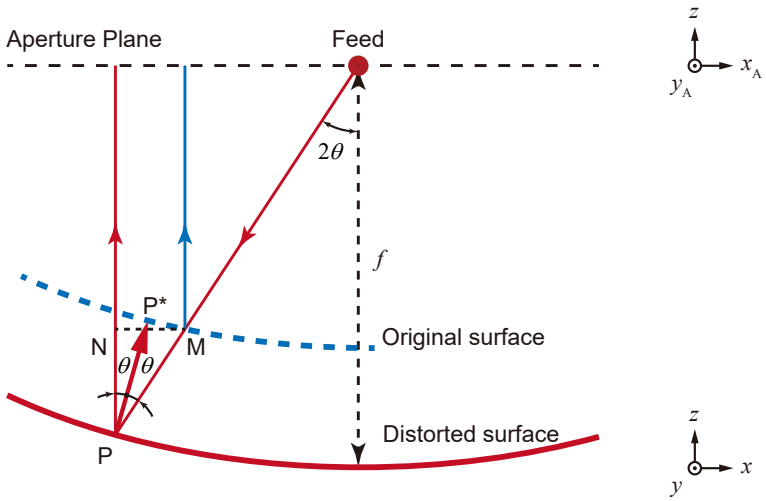

Fig. S1. Surface distortion geometry.

2. THE TRAINING FOR THE RCNN MODEL WITHOUT PRE-TRAINING

To validate the importance of transfer learning, the RCNN model is trained directly on the data generated by GRASP Ticra 9.0 without any pre-training. Note that the same test dataset is utilized to demonstrate the reconstruction performance. The corresponding RMS error over the test dataset versus the number of training image sets used is shown in Fig. S2. It can be seen that the inverse mapping relationship is well fitted when at least 6,000 image sets are used as the training dataset. In this situation, it is extremely difficult to collect so much experimental data to perform supervised learning. In contrast, after pre-training, only 400 image sets are needed to perform transfer learning, which greatly facilitates the practical application of this method.

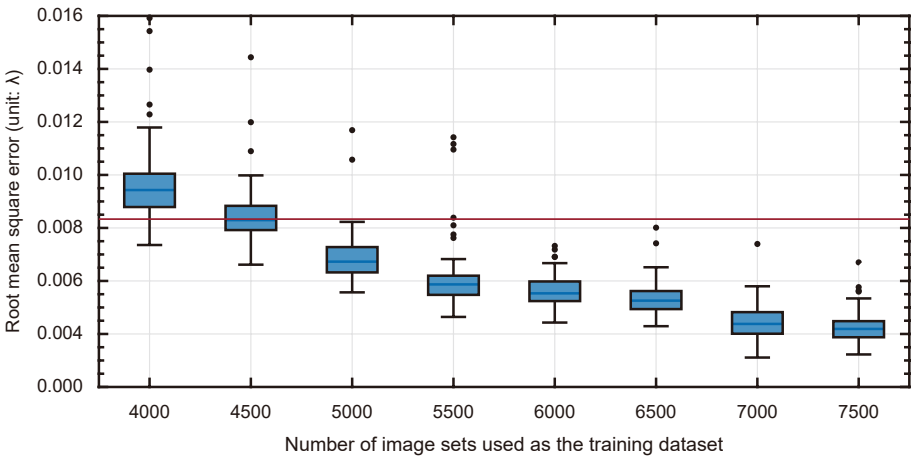

Fig. S2. Boxplots of the RMS errors of the surface reconstruction over the test dataset using the RCNN model without pre-training. The red line is the adopted accuracy criterion (RMS $<$ $\lambda/120$).

3. THE DENOISING OF THE RCNN MODEL TO POISSON NOISE

Similar to the study of Gaussian noise, Poisson noise is added to the intensity images. Then, the same test dataset consisting of 100 noisy image sets is adopted to demonstrate the reconstruction performance, and the corresponding RMS errors are shown in Fig. S3. It is clear that the performance of the RCNN model is significantly improved by noise-learning compared to its noise-free counterpart, which is in good agreement with the results under Gaussian noise. Figure S4 shows the reconstructions by different methods under noisy conditions. It is clear that the RCNN model has the best reconstruction performance under noise-learning.

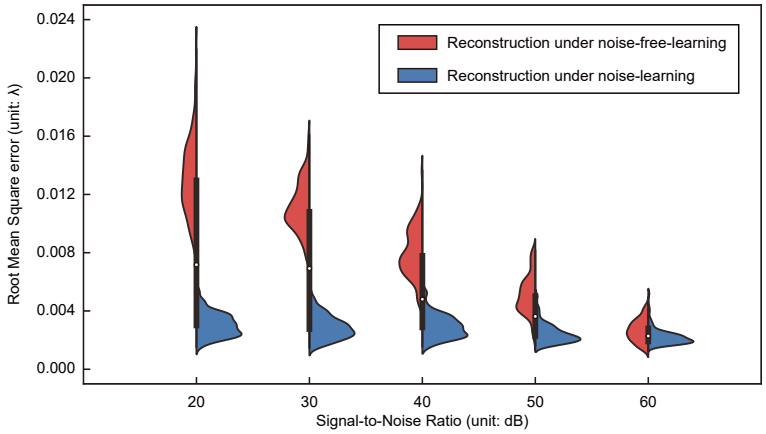

Fig. S3. The violin plots of the RMS errors of the surface recovery over the same test dataset via the RCNN model under the noise-learning and the one under the noise-free-learning.

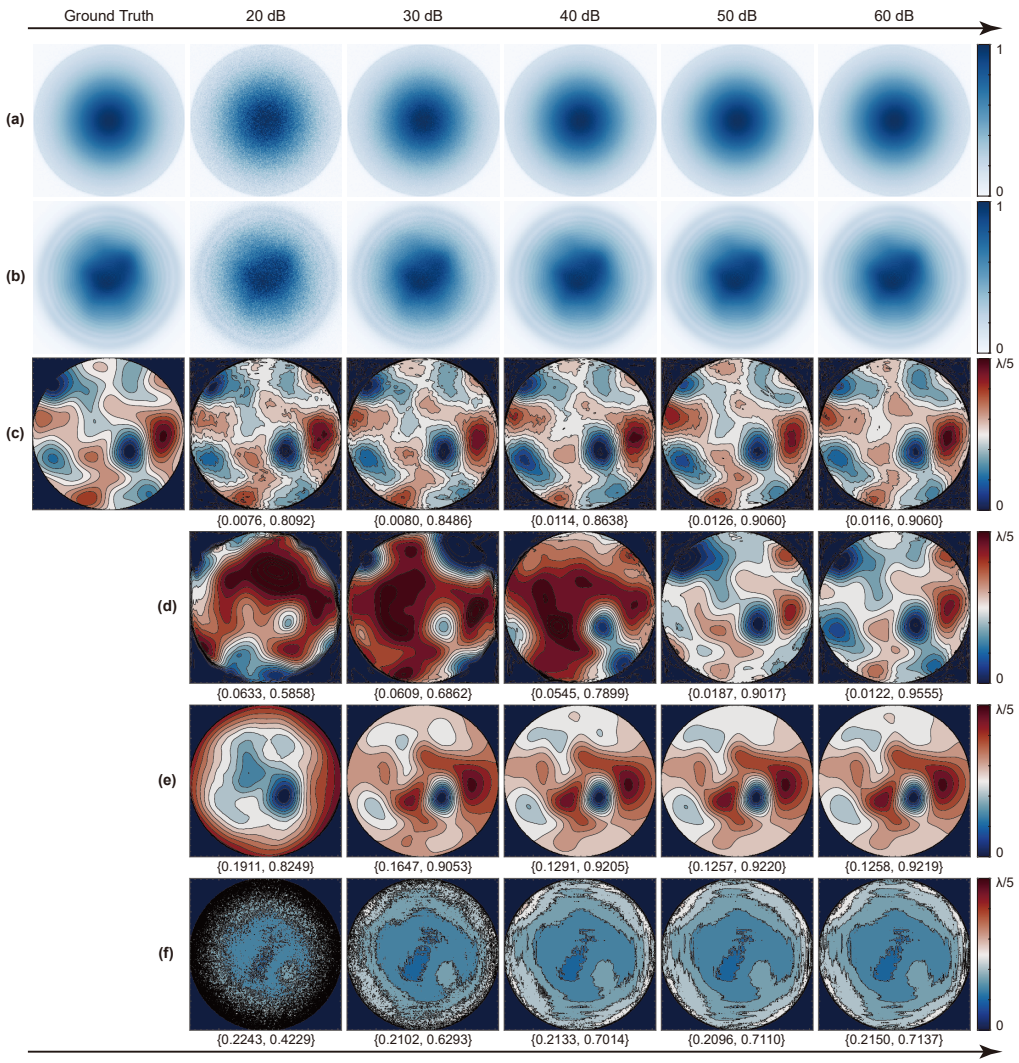

Fig. S4. Reconstruction performance of different methods under noisy conditions. (a)-(b) Original intensity image and the noisy ones at the aperture plane and at the near-field plane. (c)-(d) Surface recovery via the RCNN model under noise-learning and noise-free-learning. (e)-(f) Surface recovery via the Huang algorithm and the GS algorithm.